MOVE-III AND DEDRA: IN-SITU SUB-MILLIMETRIC SPACE DEBRIS AND MICROMETEOROID DETECTION AND CHARACTERISATION

Allan G. Schweinfurth[1], Paul Pucknus[2], Felix S. Firmbach[3], and Nicolas Zorbach[4]

[1]*School of Natural Sciences - Technical University of Munich, 85748 Garching,*
Email: allan.g.schweinfurth@tum.de
[2]*School of Natural Sciences - Technical University of Munich, 85748 Garching,*
Email: paul.pucknus@tum.de
[3]*School of Computation, Information and Technology - Technical University of Munich, 85748 Garching,*
Email: felix.firmbach@tum.de
[4]*School of Computation, Information and Technology - Technical University of Munich, 85748 Garching,*
Email: nicolas.zorbach@tum.de

ABSTRACT

The Munich Orbital Verification Experiment (MOVE) is a student CubeSat development project housed under the Scientific Workgroup for Rocketry and Spaceflight (WARR) of the Technical University of Munich (TUM). Following three successful 1U CubeSat missions, MOVE-III is currently under development and represents the fourth CubeSat mission and the first 6U mission of the MOVE project. It is supported by the MOVE-BEYOND CubeSat bus and equipped with a scientific payload consisting of two baseline and one advanced DEbris Density Retrieval Analysis (DEDRA) plasma ionisation sensors. The mission's objective is compiling a dataset of flux through in-situ observations of sub-millimetre space debris and meteoroids in Low Earth Orbit (LEO) along with object mass and speed measurements (velocity in the advanced design sensor). This dataset can be used to support the validation of the small object population of current space debris models such as ESA's Meteoroid and Space debris Terrestrial Environment Reference (MASTER) and NASA's Orbital Design Engineering Model (ORDEM) along with further space environment characterisation studies.

The DEDRA sensors are based on concepts and techniques established in the early 90s by the TUM for the Munich Dust Counter and the Mars Dust Counter. They work under the principle of impact ionisation, which generates a charge curve specific to a mass and speed combination. In addition to this, the Advanced-DEDRA design uses influential charges caused by the charged particles crossing two tilted entrance grids to determine the impact angle.

Keywords: MOVE-III, DEDRA, in-situ, space debris, detector, CubeSat, student project.

1. INTRODUCTION

Over 60 years ago, the first artificial satellite, Sputnik-I, was launched into Low Earth Orbit (LEO). This event marked the beginning of the space era. Even if the orbit of Sputnik-I decayed rapidly, for most satellites this has been the exception rather than the norm [1]. The growth of space debris has since accelerated and currently, at the dawn of the "new space" era, a reduction seems highly unlikely [2]. Undoubtedly space debris poses a threat for spaceflight. Thus a thorough characterisation of the space environment is crucial for a safe and sustainable use of space [3].

1.1. Scientific Justification

Current space models such as Meteoroid and Space Debris Terrestrial Environment Reference (MASTER) from the the European Space Agency (ESA) estimate that more than 130 million objects larger than 1 mm are currently in earth's orbit [4]. Ground based telescopes and radars are capable of tracking objects in LEO with a diameter of at least 10 cm and able of detecting and providing rough parameters for objects with a diameter as small as 1 cm, which can be used as means of population validation [5]. Particles with less than 1 cm include both space debris and micrometeoroids. They are harder to keep track of, yet still pose a considerable risk. An example of the damage a sub-millimetric particle impact can cause, can be seen in the recent events involving the Soyuz MS-22. On December 15, 2022 a sub-millimetric puncture in the external radiator cooling loop was detected. According to ROSCOSMOS, this was caused by meteoroid impact. The coolant leak resulted in the spacecraft being unable to perform mission return and a new Soyuz (MS-23) being sent to perform mission return [6].

The reduced trackability in the sub-millimetric realm

results in a more complicated validation procedure for space debris populations, as direct observation can't be used. In the case of MASTER, returned surfaces were used for the validation of this "small object population". These returned surfaces are solar arrays of the Hubble Space Telescope (HST), the Long Duration Exposure Facility (LDEF) and the European Retrieval Carrier (EuReCa). Due to the limited amount of surfaces as well as their limited time in orbit and low altitudes, extrapolation to different altitudes and times results in deviations [7]. In the sub-millimetric realm discrepancies of several orders of magnitudes arise when comparing MASTER to NASA's Orbital Debris Engineering Model (ORDEM) [8]. An additional method for population validation is active *in-situ* detection. This has been previously performed in LEO by missions such as DEBris In-orbit Evaluator (DEBIE) and more recently by Austrian Debris Detection LEo Reconnoiter (ADLER-1). However the data products from these missions have not yet found their way to the MASTER model. The data from the DEBIE detector was considered to be more than 99% noise and false positives [9] while the ADLER-1 mission is still underway [10].

The Munich Orbital Verification Experiment III (MOVE-III) is a 6U CubeSat under development at the Scientific Workgroup for Rocketry and Spaceflight (WARR) of the Technical University of Munich (TUM). Equipped with three DEbris Density Retrieval Analysis (DEDRA) plasma ionisation sensors (two baseline and one advanced sensor) the mission aims at acquiring in-situ observations of sub-millimetric space debris and meteoroids in LEO, with the objective of compiling a dataset of flux, as well as object mass and speed measurements (velocity in the advanced DEDRA design) that can be used for, but not limited to, the validation of the small object estimates of space debris populations such as MASTER and ORDEM.

This work focuses on the DEDRA sensor and its scientific objectives and the expected flux to be detected, as well as the MOVE-III CubeSat.

2. MISSION OVERVIEW AND TIMELINE

The MOVE-III mission is planned to launch no earlier than late 2024. An actual launch date has not been determined yet. An orbital altitude of 575 km at a sun synchronous orbit, with an inclination of around 97° are targeted.

The MOVE-III mission is expected to undergo four main operation phases.

- **Early Operations Phase:** begins with the CubeSat's injection into LEO. Followed by the deployment of the antennas and relevant mission initiation tasks. (First heart beat signal, flap panel deployment, etc.)
- **Commissioning Phase:** The satellite will be detumbled and all subsystems commissioned and tested. Background orbital noise in the sensors will be recorded for trigger threshold calibration.
- **Nominal operations Phase:** Data from the sensors will be recorded and transmitted to ground with position and time data. This phase should conclude at latest one year after orbital injection. If viable, it should be extended, with an expected maximum length of 5 years.
- **Decommissioning Phase:** After starting this phase, the Attitude Determination and Control System (ADCS) will be shut down, causing the satellite to tumble randomly and increases its drag cross section, thus accelerating de-orbiting. If possible, telemetry data should still be downlinked.

A full space debris mitigation analysis including deorbiting, breakup, reentry, and damage assessments has been performed [11], proving the mission is compliant with the latest IADC Space Debris Mitigation Guidelines [12]. However a further analysis shall be performed to evaluate compliance of the mission with the Federal Communications Commissions new 5-year deorbiting guildelines [13].

The mission is presently expected to be controlled from TUM's Department of Aerospace and Geodesy's mission control facilities in Ottobrunn near Munich.

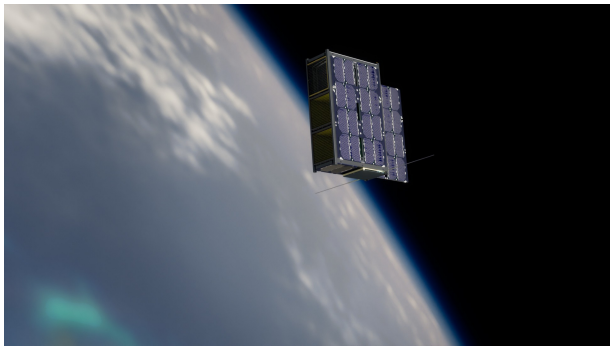

Figure 1. Concept Render of MOVE-III in Space

3. DEBRIS DENSITY AND RETRIEVAL ANALYSIS (DEDRA) SENSORS

The goal of the DEDRA sensor is to measure space debris and micrometeoroids in Low Earth Orbit with a mass from 10^{-15} kg to 10^{-10} kg and speed ranging from 7 km/s to 30 km/s. Additionally the impact direction will be measured with the Advanced DEDRA sensor. The expected power budget is 4 W for all three sensors. The two baseline sensors have a size of roughly 97 x 87 x 85 mm and a mass of 480 g. In comparison the Advanced Design is 50% longer with a mass of roughly 600 g.

3.1. Legacy

The DEDRA sensor is based on the Munich Dust Counter (MDC) and Mars Dust Counter which were developed at the Chair of Astronautics (LRT) at TUM.
The Munich Dust Counter was first launched in 1990 as part of the Japenese HITEN satellite mission to a highly elliptical earth orbit to measure measure mass and speed of micro-meteoroid particles. In total it detected 348 events averaging of about 0.5 impacts per day during the first two years of operation [14, 15].
As part of the Bremsat Mission (1994) another iteration was deployed to a 350 km circular earth orbit to detect micro-meteoroid and man-made debris from particles. This was not successful due to massive interference, originating from atmospheric particles, causing the MDC experiment at 300 km to be unsuccessful [14]. In 1998 the Mars Dust Counter was part of the NOZOMI mission to detect dust rings around Mars. Unfortunately, NOZOMI failed to enter the orbit around Mars, and the mission was abandoned in December 2003 [16, 17, 18].
The principle and the theoretical background of the mass and speed derivation is well established and consistent between the three missions that carried the MDC. But atmospheric interference can lead to major problems.

3.2. Noise Considerations

In-situ space debris detectors are often affected strongly by noise. This was the case with the GORID and DEBIE detectors [9]. A careful study of the sources and effects of orbital noise in the DEDRA sensors is being performed. The source of this noise and their intensity varies greatly. The currently identified noise sources include:

- **Electronic Noise:** This is noise from the electronic components of the charge amplifying circuit. This is addressed with help of low-pass filters and the use of low noise components.
- **Charged Particles:** Ionised atoms and particles that can trigger false-positives can be found in the space environment. The spatial distribution of these particles is difficult to predict as it varies location, time, and date. There exist current models such as International Reference Ionosphere Model (IRI), that can be used to predict the amount of charged particles to be encountered [19].
- **Photoelectrons:** Solar radiation can rip off electrons from the inside surface of the sensor box. This source is to be addressed during the calibration campaign by simulating the solar environment. Additionally, the noise levels with different solar illumination angles, can be recorded during the commissioning phase and be used for data post processing and trigger setting.
- **Induced Electromagnetic Fields:** Fields induced by components of the satellite such as magnetorquers, reaction wheels and their interaction with the earth's magnetic field can induce electric fields that can influence the sensor's measurements. This is to be addressed during the calibration campaign.

3.3. Operating Principle

The measurement is based on the principle of impact ionisation. Particles from space entering the sensor will collide with any surface inside the box. Due to the high impact speed the particle is partially ionised in a plasma composed of positive and negative ions. The amount of charge generated increases with mass and speed. Above a speed of 5 km/s a substantial amount tuns into a plasma cloud [20, 21]. The resulting charges will then be attracted and trapped by two Charge Trap Plates (CTP), one having a high positive potential (+180 V) and the other having a high negative (-180 V) potential. At the entrance of the sensor box, two grids with a potential of 0 V are placed, to reduce the effect of external electromagnetic fields. The inner walls and bottom of the sensor are coated in gold to achieve a maximum charge gain after impact. These surfaces are also set to a potential of 0 V. Both collector plates, the entrance grids, and the bottom impact plate are connected to separate charge amplifiers. Resulting in four separate measurements channels. These channels are the Electron Channel (EC), the Ion Channel (IC), the Entrance Grid (Grid), and the Neutral Channel (NC). A schematic drawing of the baseline as well as advanced sensor, including the different channels, can be seen in in Figure 2.

Qualitative impact signals from all four channels, plotted as charge curves, can be seen in Figure 3. The shape of

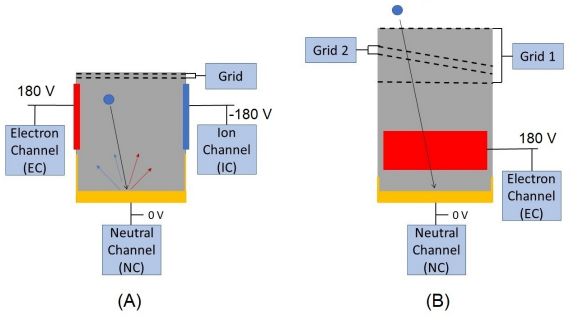

Figure 2. Schematic drawing of the (A) DEDRA Baseline and (B) Advanced Design. To highlight the grid structure the schematic of the Advanced Design is rotated 90 degrees in relation to the Baseline. The red rectangle represents the Electron Channel biased at +180 V and the blue one the Ion Channel biased at -180 V. The yellow area represents the Neutral Channel that is connected to to common satellite ground. The dotted lines represent the entrance grids which are also connected to ground. The blue circle represent an impactor and the arrows the resulting charges after impact (blue: negative, red: positive). Charge measurements will be done on the EC, IC, NC and grids respectively.

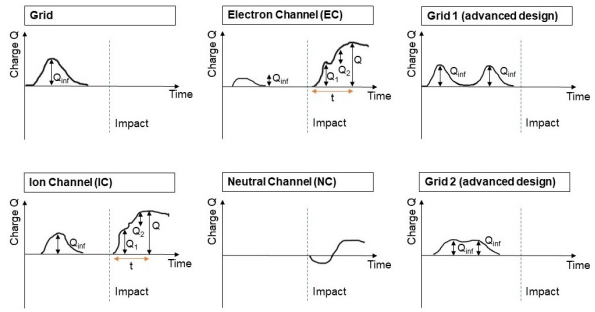

Figure 3. Qualitative drawing of the charge measurements of the different channels. The x-Axis represents time while the y-Axis displays the measured charge. t represents the time between impact and maximum charge, Q_{inf} the maximum charge from electrostatic induction, Q the overall maximum charge and Q_1 and Q_2 the primary and secondary charge. Grid 1 and 2 are the grid charge signals from the Advanced Design.

the curves vary for different speeds and mass as well as the path and impact location of the particle. The difference between the amount of charge detected at the channels after an impact, as well as the time delay between the detection on the channels provide information on the impact location of the particle. In order to derive speed and and mass of a collided particle following empirical equations can be used [21]:

$$\left.\begin{aligned} v^{ch} &= C_t^{ch} t^{\eta^{ch}} \\ v^{ch1,ch2} &= C_{dt}^{ch1,ch2} dt^{\kappa^{ch1,ch2}} \\ v^{EC} &= C_{12}^{EC} (\tfrac{Q_1}{Q_2})^{\delta^{ch}} \end{aligned}\right\} v_{mean;ch=IC,EC,NC} \tag{1}$$

where t is the rise time until maximum charge, dt the time delay between charge gain of IC and EC, Q_1 the primary charge, Q_2 the secondary charge and Q the maximum charge of the channel. The constants (C_i^{ch}, β, η, κ, δ) will be derived from the data obtained during the calibration campaign. Once the velocity for each channel (EC, IC and NC) has been calculated, a mean value v_{mean} can be derived. Using the mean velocity the mass of the particle can be determined [21]:

$$m_{ch} = \frac{Q^{ch}}{C_\rho^{ch} v_{mean}^{\beta^{ch}}} \Rightarrow m_{mean} \tag{2}$$

Again the mass estimation will be done for each channel, based on the channel-specific charge and calibration parameters. Later the average of all channels will be calculated. Based on the signal slope and amplitude, a trigger logic continuously evaluates weather or not an impact has occured.

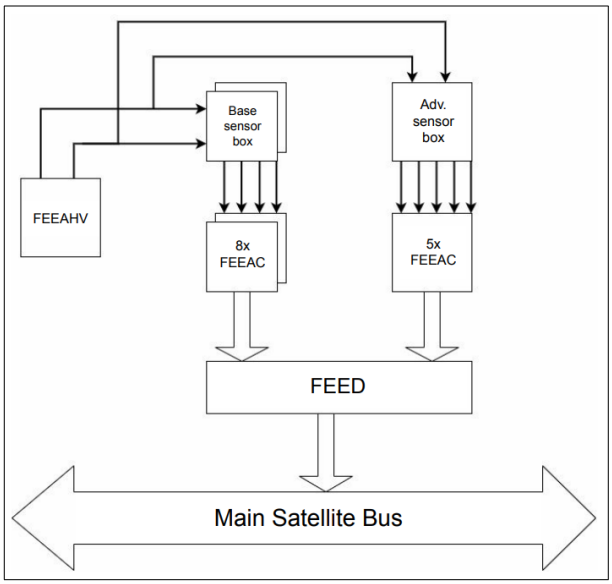

Figure 4. High level architecture of the scientific payload of MOVE-III.

3.4. Architecture

The scientific mission's payload consists of two baseline and one advanced DEDRA sensors. The electronics is divided up into three subsystems. The High-Voltage Analogue Front End Electronics Circuit (FEEAHV) circuit generates a high positive and negative voltage that will be applied to the CTPs. One Front End Electronics Alternating Current (FEEAC) circuit for each measurement channel will amplify the charge signals. For each baseline sensor there will need to be four similar FEEAC circuits while there will be five for the advanced sensor. The Front End Electronics Digital (FEED) subsystem will digitise the data of all FEEACs, process it and put it on the main satellite bus. FEED will consist of multiple Analog to Digital Converters (ADCs), a Field Programmable Gate Array (FPGA) as the processing unit, a microcontroller and an Static Random-Access Memory (SRAM) to buffer data. The architecture of the payload can be seen in Figure 4.

The mass of each baseline sensor is 480 g. The sensor has a aperture of 97 x 87 mm and a depth of 85 mm. Furthermore one PCB, housing the charge amplifying circuit, will be mounted to the bottom of each sensor while the digital processing circuit FEED will be placed on a PCB that is directly attached to the satellites backplane.

The entrance grids consist of bars with a diameter of 0.1 mm. The spacing between the grid lines is 4 mm. The grid will be etched from a solid sheet of metal and later coated in gold. An aluminium frame will hold the grids in place. The $\pm$180V at the CTPs is generated by the Front End Electronics Analogue High Voltage (FEEAHV) based on a flyback circuit. At each measurement channel the signal is first processed by the Front End Electronics Analogue Circuitry (FEEAC). The in-

coming signal is amplified by a charge sensitive amplifier and then compressed by a logarithmic amplifier. The analogue signal will be continuously converted to digital by an analogue-to-digital converter at five Mega Samples Per Second (MSPS) and a bit depth of ten. This approach results in 500 sample points during a 100 μs period of interest. The digital output is handled by Front End Electronics Digital (FEED) based on an FPGA and microcontroller. The digital trigger logic continuously checks whether an impact has occurred or not. After an impact has been detected, the data 270 μs before and after impact detection will be stored for each channel of the corresponding sensor. Together with the sensor number, attitude, position and time information, the impact data is stored as a science data package and transferred to the Command and Data Handling (CDH) data storage. Finally, the package will be transmitted to the ground station via the Communications (COM) module.

3.5. Advanced Design

The Advanced DEDRA Sensor shall be capable of simultaneously measuring mass, speed and impact direction of incoming particles. The concept employs two additional tilted grids, identical in design with the grids of the baseline design, placed in between two parallel ones. In order to accommodate the extra grids, the advanced design sensor is roughly 50% longer than the baseline design sensor and has a increased mass of 601 g. The tilted grid is rotated by an angle of $\epsilon = 15°$ around the axis perpendicular to the CTP. A schematic of the complete grid assembly can be seen in Figure 2.

The advanced sensor concept measures the charge on all entrance grids. Particles in space carry a small electrical charge, which results in a charge gain on the entrance grids due to electric induction. By determining the time at which the particle passes through the each of the grids, the Cartesian velocity vector (v_x, v_y, v_z) of the particle can be calculated using the equations of motion. The components of the Cartesian velocity vector can be derived as shown in Eqs. 3-5:

$$v_z = \frac{h_4 - h_1}{t_4 - t_1} \tag{3}$$

$$v_x = \frac{\frac{h_3 - h_2}{t_3 - t_2} - v_z}{\tan(\epsilon)} \tag{4}$$

$$v_y = \pm\sqrt{v^2 - (v_x^2 + v_z^2)} \tag{5}$$

where t_i is the time at which the particle is inside grid i, h_i the height of grid i with respect to the impact plate (for the tilted grid the higher side is used), ϵ tilted grid angle and v the speed determined as described in the operating principle section.

From the velocity vector components, the angles of incidence θ and ϕ can then be derived as shown in Eqs. 6-8. Due to the fact that v_y is ambiguous there are two possible solutions for ϕ. The ambiguity, which comes from the fact that v_y is derived from the absolute velocity v and the components v_x and v_z, can be resolved by utilising the charge differences recorded on the right and left CTPs.

$$\theta = \arccos\left(\frac{v_z}{v}\right) \tag{6}$$

$$\phi_1 = \arctan\left(\frac{v_y}{v_z}\right) \tag{7}$$

$$\phi_2 = 2\pi - \phi_1 \tag{8}$$

3.6. Mechanical

The baseline sensor has dimensions of 97 x 87 x 85 mm with a mass of 480 g. While the Advanced Design is 50% longer and weighs 601 g. A CAD drawing of the baseline sensor design can be seen in Figure 5. The sensors will be constructed from milled aluminium plates. The box is formed by screwing the sheets together. The inside walls will be coated in a gold layer with a few microns of thickness. All grids are manufactured in the same manner by etching the structure from metal sheets and coating them in gold afterwards. The grid strands have a thickness of 0.1 mm and a spacing of 4 mm. These will be held in place by an aluminium frame that will be screwed to the overall structure. The EC and IC are made from additional pieces electrically isolated from the rest of the structure. They will be located centred in the upper half of the sensor on opposing sides. They are 90% as wide as the interior width and 45% as high as the interior height.

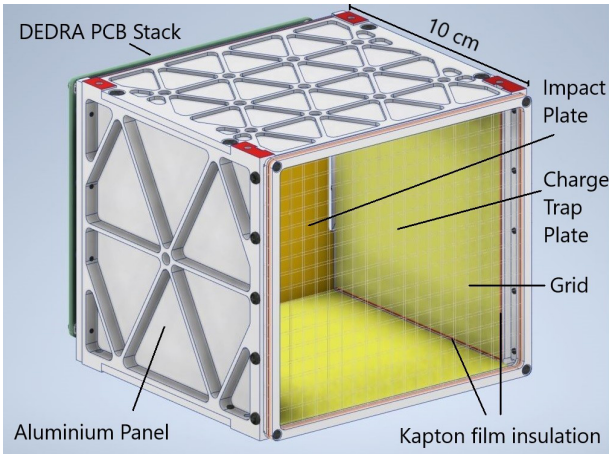

Figure 5. CAD rendering of the Baseline DEDRA Sensor with labelled components.

3.7. High-Voltage Analogue Front End Electronics Circuit (FEEAHV)

The High-Voltage Analogue Front End Electronics (FEEAHV) is a voltage regulating circuit which generates a high voltage in order bias the electron and Ion collector plates. A constant voltage of +180 V for the electron detector and -180 V for the ion detector will be used. These voltages were derived from the Munich Dust Counter. The power consumption of the FEEAHV circuit should be kept as low possible. After considering and simulating several options containing an off-the-shelf voltage regulator a custom made flyback circuit was designed. Circuit simulations showed that the custom flyback circuit is able to generate the intended voltage while having a considerably lower power consumption. A flyback converter consists of two isolated circuits that use a transformer to transfer energy from the primary circuit into the secondary. In the primary circuit a Metal-Oxide-Semiconductor Field-Effect Transistor (MOSFET) is switched in order to magnetise and demagnetise the transformer. The switch is driven by a 555 timer in a stable mode. In the secondary circuit a capacitor gets charged to a voltage of 180V through a rectifying diode.

3.8. Front End Electronics Alternating Current (FEEAC)

The charge signal created by the impact is amplified in the Front End Electronics Alternating Current (FEEAC) circuit. Each baseline sensor will have four FEEAC circuits as there are four channels. The advanced sensor will have one additional for the tilted grids. The circuits will be fundamentally the same but some adaptations need to be done depending one the polarity of the charges that are supposed to be amplified. This circuit is required to convert a high dynamic range of charge from 10^{-14} C to 10^{-9} C into voltage and condense this voltage range in order to achieve an equally good resolution for small charges and large charges. Furthermore the noise charges caused by photoionisation inside the sensor box and by the charges the sensor will collect while orbiting in the ionosphere must be filtered. But not only external noise can be problematic for the FEEAC also electronic noise can deteriorate the quality of measurements of small impacts.

The front-end of the current design consists of a transimpedance amplifier and a charge amplifier with a input resistor. The external noise is filtered in front of the charge amplifier by subtracting the signal of the same channel of one of the other two sensors from the voltage signal behind the transimpedance amplifier. The output of the charge amplifier is then feed into the a CMOS switch and a comparator. The comparator is supposed to turn the switch on if the voltage is positive and off if the voltage is negative in order protect the input of the logarithmic amplifier from negative voltages. A logarithmic amplifier can only handle positive inputs. The off-the-shelf logarithmic amplifier LOG114 from Texas Instruments is used to condense the signal. It has a high dynamic range and internal temperature compensation. After that the signal is temperature compensated for the second time and shifted to fit inside the analogue input range of the Analogue to Digital Converter (ADC).

3.9. Digital Front End Electronics (FEED)

After the charges have been amplified by the FEEAC the signals are digitised and processed in the Digital Front End Electronics (FEED). A total of 13 channels sampled at 5MSPS and with a resolution of at least 10 bits have to be processed. The objective of FEED is to discard all data that only contains noise and transfer the data that might contain an impact onto the satellite bus.

A single FPGA is in charge of the data processing due to its ability to process many data streams simultaneously. In the FPGA an amplitude trigger and a transient trigger are implemented. In case of an impact the charge signals are expected to rise above a certain amplitude threshold and have a faster rise time than noise signals. Since the noise signals can not be predicted reliably, fixed thresholds might lead to too many false positives. For this reason the threshold have to be configurable in orbit. If an impact occurs the trigger is deployed and around 270 μs of data before and after the deployment of the trigger is saved from the sensor where the trigger signal was caused. As there is no way of knowing when and where an impact occurs, the data of every channel has to be buffered for 270 μs. The charge data containing the potential impact together with information about which channel deployed the trigger is send to the microcontroller. This microcontroller puts the sensors data on the Controlled Area Network (CAN) communication bus and requests the current position and attitude of the satellite from the Command and Data Handling (CDH) and Attitude Determination and Control System (ADCS) subsystems respectively.

In order to not be restricted to only FPGAs with large internal memories and to simplify the interface to the satellite bus, the data storage is outsourced to a dual-port SRAM. A ring buffer is implemented on this SRAM. Seven two-channel successive approximation (SAR) ADCs with a sampling rate of 5MSPS and a resolution of 16 bit are likely going to be used in order to digitise all channels. The complete architecture of FEED can be seen in Figure 6.

The data package that contains all the valuable information about a potential impact is called the Science Data Package. Its largest part is made up by the charge data. In the current design the data package contains four channels with 540 μs of data sampled at 5 MSPS at a resolution of 12 bits. This amounts to 16.2KB. Additionally the number of the channel and sensor belong to the Science Data Package as well as attitude and position of the satellite at the moment of the trigger.

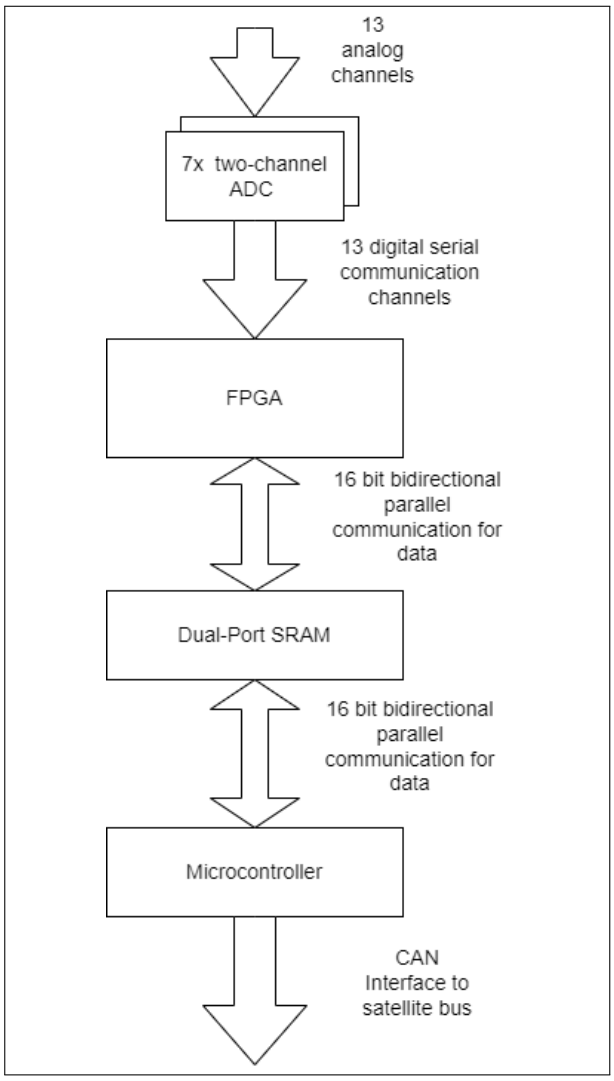

Figure 6. Architecture of FEED

3.10. Calibration

The Calibration campaign is planned using an electrostatic particle accelerator [22]. Particles of known mass and velocity will be shot at different locations inside the sensor box. Together with the corresponding impact data, the calibration constants will be determined. The scope of the campaign not only includes determination of the calibration constants but also to quantify on-ground noise level to further help differentiating signals from noise and particle impacts when the detector operates in space. Additionally the measurement uncertainties will be quantified by analysing the calibration results. Based on the performance of the MDC on Nozomi, maximum error factors of 1.5 and 5 are expected for the speed and mass measurements respectively [21, 16].

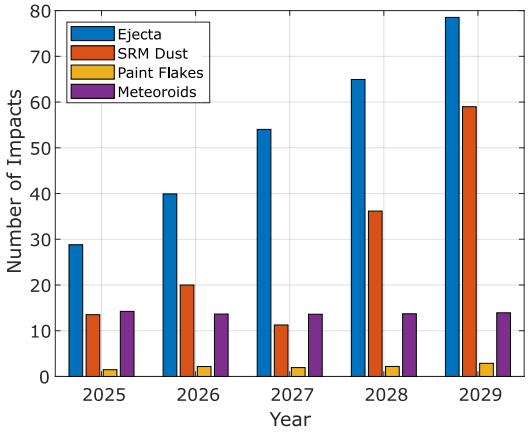

Figure 7. Annual number and type of impactors during the extended operational phase at an orbital altitude of 575 km. Obtained using MASTER 8.0.3.

4. EXPECTED SPACE DEBRIS AND METEOROID FLUX

The flux of space debris and meteoroids expected in the target orbit of 575 km was estimated with MASTER 8.0.3. For a launch in 2024 with an extended nominal operations phase of 5 years, an average impactor rate of around 97 impactors with a mass between 10^{-15}kg and 10^{-10}kg per year is estimated for a cross section of 8178 mm^2 which corresponds to the 3 DEDRA sensors. These impactors include human made particles and meteoroids following the Grün meteoroid model with a Taylor velocity distribution [23]. The most abundant human made particles altitude at MOVE-III's are ejecta, Solid Rocket Motor (SRM) dust, and paint flakes. The remaining types of particles found in the master populations are negligible, as their flux is ≈ 0. The evolution of the number and type of impactor can be seen in Figure 7. This values can change depending on the actual launch date.

5. MOVE-BEYOND PLATFORM

5.1. Overview

The DEDRA sensor will be supported by the MOVE-BEYOND bus, also developed by the MOVE team supported by the Chair of Astronautics, and the Chair of Pico- and Nanosatellites and Satellite Constellations of TUM. There are several versions of the bus capable of supporting 1U, 2U, 3U and 6U CubeSats.

MOVE-BEYOND provides the payload with a CAN-bus connection to other subsystems and access to the Command and Data Handling subsystems MRAM data storage. The Electrical Power System delivers 3.3 V, 5 V and unregulated battery power (7.4–8.4 V) as well as electrical safeguards such as an overcurrent protection. In the

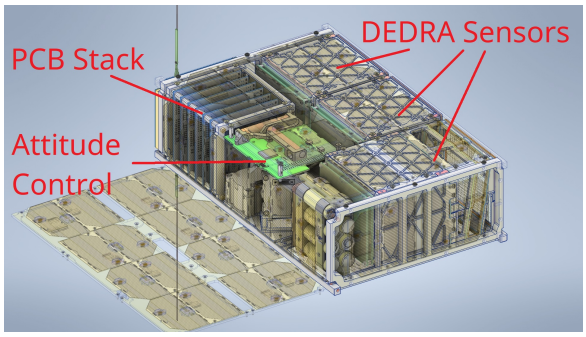

Figure 8. MOVE-III Rendering. Note the sensor boxes, which take up 1U. The space behind the larger Advanced Design Sensor (1.5U) contains optional, additional batteries.

configuration chosen for MOVE-III, it offers 20.8 Wh of battery storage. The Attitude Determination and Control system is capable of pointing the satellite with a precision of 3° using four reaction wheels as well as in-house-developed magnetorquers. A downlink of 9600 bps is provided via a 437 MHz UHF communications module.

Data storage capacity is offered through the bus' Command and Data Handling subsystem, containing a 4 GBit octal SPI MRAM chip. Discouting space for housekeeping and system telemetry data, the effective data storage is limited to 300 MB [24]. Assuming a size of 16.2 KB per Science Data Packets (section 4.9), this amounts to roughly 18000 packets storable on-board.

The bus runs on an in-house operating platform, the Distributed Operation System Initiative for Satellites (DOSIS). It enables every subsystem to run its own operating system instance, for which the University of Würzburg's open-source OS, RODOS, was chosen. DOSIS provides every subsystem with standardised device/daemon interfaces, as well as time synchronisation [25], which is used to establish time of impact in the Payload's data product.

5.2. Configuration

The payload will communicate with the bus via a specialised circuit board that will fit into the bus' PCI standard connectors, located in the PCB stack.

The mission requires a minimum of three sensors to increase the sensing area and maximise impact likelihood. Each sensor is 1U in size. Therefore, a 6U CubeSat configuration is needed to host both bus and sensors. There are multiple options for sensor placement. The bus itself will require 2U, 1U for the PCB stack containing the board computer as well as batteries and the data bus, and 1U for the Attitude Control system. Figure 8 shows a render of the current configuration. Note the three boxes, which are the DEDRA sensors. The larger box is the Advanced sensor.

5.3. Testing

Both sensor and bus will undergo a testing campaign in compliance with the ECSS-E-ST-10-03 standard published by ESA [26]. This campaign will include unit tests of the sensors and the bus subsystems as well as integrated tests. Evaluation of failure modes and Thermal Vacuum (TVAC) tests will be performed. The calibration campaign described in section 4.10 will ideally be performed when the sensor is connected to the bus.

6. CURRENT STATUS

The MOVE-III mission has passed its Preliminary Design Review (PDR) as of February 2022. Breadboard-level prototyping has largely been completed. Presently, the team is engaged in creating a first integrated model of the satellite called the Extended Brass Model, envisioned to bring all subsystems - including the payload - to a testable level. Flight hardware will be installed after the initial testing campaign finishes, and the tests will be repeated thereafter. A launch will occur no earlier than 2024.

All electrical subsystems of payload have been successfully simulated. Before the calibration campaign, which is planned for late 2023, the hardware has to be designed and tested, the sensor box has to be manufactured and the interface to the satellite bus has to be implemented.

7. ACKNOWLEDGMENTS

We would like to thank all university students and staff involved in the MOVE project, the TUM Chair of Astronautics (LRT), Chair of Aerospace and Geodesy (ASG), and Chair of Pico- and Nanosatellites, and Satellite Constellations, the German Aerospace Center (DLR) and Freunde der TUM e.V for their support.

REFERENCES

1. Royal Astronomical Society, (1959). Artificial Satellites: I. The Motions of Artificial Satellites, *Monthly Notices of the Royal Astronomical Society*, **119**(4), 424–432
2. Schaus V., Letizia F., Bastida Virgili B., et al., (2021). Leveraging space debris simulation results: Revisiting guideline values for explosion and cumulative collision rate, *Proceedings of the 8th European Conference on Space Debris*, ESA
3. Krisko P.H., (2007). The predicted growth of the low-Earth orbit space debris environment — an assessment of future risk for spacecraft, *Proceedings of the Institution of Mechanical Engineers, Part G: Journal of Aerospace Engineering*, **221**(6), 975–985

4. European Space Agency, (2022). Space Environment Statistics

5. Merholz D., Leushacke L., Flury W., et al., (2002). Detecting, Tracking and Imaging Space Debris. Space Environment Statistics, *ESA Bulletin*, **109**(1), 128–134

6. State Corporation Roscosmos, (2023). Soyuz MS-22: the decision of the state commission (Telegram Release), https://t.me/roscosmos_gk/8095

7. Braun V., (2019). Impact of Debris Model Updates on Risk Assessments, *Proceedings of the 1st NEO and Debris Detection Conference*, ESA

8. Horstmann A., Manis A., Braun V., et al., (2021). Flux Comparison of Master-8 and Ordem 3.1 Modelled Space Debris Population, *Proceedings of the 8th European Conference on Space Debris*, ESA

9. Bunte K.D., Jurke K.-N., (2021). Data of European in-situ Impact Detectors for Environment Model Validation, *Proceedings of the 8th European Conference on Space Debris*, ESA

10. Groemer, G., (2021). ADLER-1 In-situ Space Debris Measurements, *Presentation at MASTER Modelling Workshop*, ESA

11. Oikonimidou X., Karagiannis E., Schweinfurth A.G, Firmach F.S, Pucknus P., et al., (2022). MOVE-III: A CubeSat for the detection of sub-millimetre space debris and meteoroids in Low Earth Orbit. *Frontiers in Space Technologies*

12. Inter-Agency Space Debris Coordination Committee (IADC), (2020). Space Debris Mitigation Guidelines, IADC

13. Federal Communications Commission (2022). FCC22-74, https://docs.fcc.gov/public/attachments/FCC-22-74A1.pdf

14. Igenbergs E., Hüdephol A., Uesugi K., Hayashi T., et al., (1991). The Present Status of the Munich Dust Counter Experiment on Board of the HITEN Spacecraft, *International Astronomical Union Colloquium*, **126**(1), 15–20

15. Iglseder H., Münzenmayer R., Svedhem H., Grün E., (1993). Cosmic dust and space debris measurements with the Munich dust counter on board the satellites hiten and brem-sat, *Advances in Space Research*, **13**(8), 129–132

16. Sasaki S., Igenbergs E., Ohsashi H., et al., (2002). Observation of interplanetary and interstellar dust particles by Mars Dust Counter (MDC) on board NOZOMI, *Advances in Space Research*, **29**(8), 1145–1153

17. NASA, (2022). Space Science Data Coordinated Archive - 1998-041A - Nozomi, https://nssdc.gsfc.nasa.gov/nmc/spacecraft/display.action?id=1998-041A,

18. Biswal M., Annavarapu R. M., (2019) Mars Missions Failure Report Assortment: Review and Conspectus, *AIAA Propulsion and Energy 2020 Forum*

19. Committee on Space Research (COSPAR) and International Union of Radio Science (URSI), (2016). International Reference Ionosphere Model

20. Hofschuster G., (2002). Hochgeschwindigkeitseinschläge auf teildurchlässige Oberflächen , Dissertation at Technical University of Munich

21. Senger R., (2008). Data Handling and Evaluation for Autonomous Experiments in Interplanetary Missions, *Planetary and Space Science*, **56**(7) 1057–1059

22. Mocker A., Albin T., Gruen E., et al., (2019). The Hyper-Velocity Dust Research Laboratory at the Institute for Space Systems at the University of Stuttgart, *EPSC-DPS Joint Meeting 2019*

23. European Space Agency, (2022). Software User Manual - MASTER, https://sdup.esoc.esa.int/master/downloads/documentation/8.0.3/MASTER-Software-User-Manual.pdf

24. MOVE (2022). Preliminary design review (PDR) of the MOVE-III mission. *Available on Demand*

25. Rückerl S., Ukkola M., Würl S., Faehling M., (2021). Distributed Computing for Modular and Reliable Nanosatellites, *Proceedings of the 2021 IEEE Aerospace Conference*

26. European Space Agency, (2022). ECSS-E-ST-10-03C Rev.1 – Testing, https://ecss.nl/standard/ecss-e-st-10-03c-rev-1-testing-31-may-2022/